Anisotropic magnetic switching along hard [110]-type axes in Er-doped $DyFe_2/YFe_2$ thin films

G. B. G. Stenning[1,2], G. J. Bowden[1], G. van der Laan[3], A. I. Figueroa[3], P. Bencok[4], P. Steadman[4], and T. Hesjedal[5]

[1.] *School of Physics and Astronomy, University of Southampton, SO17 1BJ, United Kingdom*
[2.] *ISIS Neutron and Muon Source, Rutherford Appleton Laboratory, Didcot, OX11 0QX, United Kingdom.*
[3.] *Magnetic Spectroscopy Group, Diamond Light Source, Didcot OX11 0DE, United Kingdom*
[4.] *Diamond Light Source, Didcot OX11 0DE, United Kingdom*
[5.] *Clarendon Laboratory, University of Oxford, OX1 3PU, United Kingdom*

Abstract

Epitaxial-grown $DyFe_2/YFe_2$ multilayer thin films form an ideal model system for the study of magnetic exchange springs. Here the $DyFe_2$ (YFe_2) layers are magnetically hard (soft). In the presence of a magnetic field, exchange springs form in the YFe_2 layers. Recently, it has been demonstrated that placing small amounts of Er into the centre of the YFe_2 springs generates substantial changes in magnetic behavior. In particular, (*i*) the number of exchange-spring states is increased dramatically, (*ii*) the resulting domain-wall states cannot simply be described as either Néel or Bloch walls, (*iii*) the Er and Dy magnetic loops are strikingly different, and (*iv*) it is possible to engineer Er-induced magnetic exchange-spring collapse. Here, results are presented for Er-doped (110)-oriented $DyFe_2(60\ \text{Å})/YFe_2(240\ \text{Å})_{15}$ multilayer films, at 100 K in fields of up to ±12 T. In particular, we contrast magnetic loops for fields applied along seemingly equivalent hard-magnetic [110]-type axes. MBE-grown cubic Laves thin films offer the unique feature of allowing to apply the magnetic field along (*i*) a hard out-of-plane [110]-axis (the growth axis) and (*ii*) a similar hard in-plane [$\bar{1}$10]-axis. Differences are found and attributed to the competition between the crystal-field interaction at the Er site and the long-range dipole-dipole interaction. In particular, the out-of-plane [110] Er results show the existence of a new magnetic exchange spring state, which would be very difficult to identify without the aid of element-specific technique of x-ray magnetic circular dichroism (XMCD).

Keywords Thin magnetic films, Magnetic exchange springs**,** Micromagnetics**,** Dipolar fields**.**

PACS number(s): 75.70.Cn, 75.60.Jk, 75.50.Vv, 75.78.Cd, 75.60.Ch, 75.50.Gg, 75.30.Gw

Authors email addresses
gavin.stenning@stfc.ac.uk
gjb@phys.soton.ac.uk (Corresponding author)
Gerrit.vanderlaan@diamond.ac.uk
adriana.figueroa-garcia@diamond.ac.uk
Peter.Bencok@diamond.ac.uk
paul.steadman@diamond.ac.uk
Thorsten.Hesjedal@physics.ox.ac.uk

1. Introduction

Switching mechanisms in thin film bits will always be of interest to the magnetic recording industry. In particular, it has been suggested that bilayer films consisting of hard and soft layers should find a role in beating the so-called superparamagnetic limit, where $KdV \rightarrow kT$, Weller and Moser [1]. Here *K* and dV are the anisotropy and change in volume, respectively, of the magnetic bit. Thus if we wish to decrease dV, it is imperative to move to higher anisotropy *K* materials. However the latter inevitably leads to an undesired need for higher write fields. This problem has been addressed by Suess *et al*., [2] and Krone *et al*., [3], who suggest combining the hard bit with a soft magnetic layer. In such bilayer systems, magnetic exchange springs set in the soft layer act as magnetic levers, thereby reducing the field required to switch the magnetic bit.

More recently, magnetic switching mechanisms have been studied in molecular beam grown (MBE)-multilayer films of the cubic Laves $DyFe_2/YFe_2$ at 100 K [4,5,6]. Such films are characterized by very sharp Dy/Y interfaces, and form a very good test bed for the study and manipulation of magnetic exchange-spring systems. Here, the $DyFe_2$ layers are hard while the YFe_2 layers are magnetically soft. Thus in the presence of an applied field, magnetic exchange springs are set up in the YFe_2 layers. Specifically, switching scenarios have been described for a $DyFe_2(60\,\text{Å})/YFe_2(240\,\text{Å})_{15}$ multilayer, for fields applied in-plane along either an easy [001]-axis or hard in-plane $[\bar{1}10]$ axis. More recently, a particular study of an Er-doped $DyFe_2/YFe_2$ multilayer has been performed, which shows that (*i*) the Er moments can be switched before those of the harder Dy layers, and (*ii*) up to 10 different exchange springs states are accessed during magnetic reversal [6]. However, all of this work has been performed with magnetic fields applied along *in-plane* easy [001] or hard $[\bar{1}10]$ axes.

Here we present results for an Er-doped (110)-oriented multilayer $DyFe_2(60\,\text{Å})/$ YFe2*(120 Å)*/ErFe2(4 Å)/YFe2*(120 Å)]15* film, again at 100 K for comparative purposes, in fields of up to ±12 T applied along an *out-of-plane* [110]-axis. Thus we are able to contrast magnetization curves for fields applied along seemingly equivalent [110] and $[\bar{1}10]$-axes. Both axes are illustrated in Fig. 1. Thin films of the cubic Laves structure offer the unique feature of allowing the magnetic field to be applied along (*i*) a hard out-of-plane [110]-axis (the growth axis) and (*ii*) a similar hard in-plane $[\bar{1}10]$-axis. In practice, differences are found in both the Dy and Er magnetic loops. In particular, the latter are attributed to competition between the predominantly cubic crystal-field interaction at the Er site, and the long range dipole-dipole interaction which confers in-plane anisotropy. In short, the out-of-plane [110] Er results reveal the existence of a new magnetic exchange-spring state $Dy_B[010]/Er_S[\bar{1}1\bar{1}]$, while its $[\bar{1}10]$ counterpart $Dy_B[010]/Er_S[11\bar{1}]$ appears to be either unstable or weakly stable and as such is bypassed by exchange spring collapse [6]. Here, the subscript B (S) in, say, the spring state $Dy_B[010]/Er_S[\bar{1}1\bar{1}]$ refers to Dy in the *bulk* $DyFe_2$ layer, Er in the *spring*, respectively (see Ref. [6] for more details and discussion).

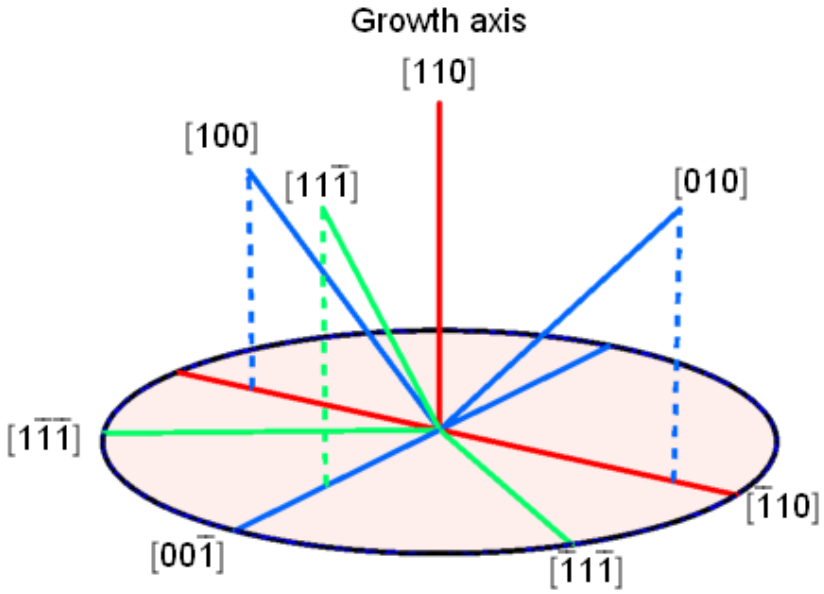

FIG. 1. The principal axes in an MBE-grown thin film of the cubic Laves phase $R\mathrm{Fe}_2$ intermetallic compound. The [110]-direction (the growth axis) is perpendicular to the plane of the film. The easy (hard) axes <100> (<110>) for the Dy ions are shown in blue (red), respectively. The easy <111> axes for the Er ions are shown in green.

Finally, we note that while this and most of the previous work has been concerned with essentially DC magnetic switching, this work will also have relevance for picosecond switching in $\mathrm{DyFe}_2/\mathrm{YFe}_2$ multilayer systems, as described by Shelford *et al.*, [7].

2. Experimental details and results

Details of (*i*) the growth of the MBE-grown 4000 Å thick films used in this work, and (*ii*) determination of both the Dy and Er magnetization loops, can be found in Wang *et al.*, [8] and Stenning *et al.*, [6], respectively, and will not be reiterated here. Once again, x-ray magnetic circular dichroism (XMCD) experiments were performed using the Er $M_{4,5}$ (1405, 1446 eV) and Dy $M_{4,5}$ (1293, 1327 eV) absorption edges, in fluorescence detection. A review of this technique can be found in Ref. [9]. A schematic representation of the experiments, illustrating the two orientations used, can be seen in Fig. (2).

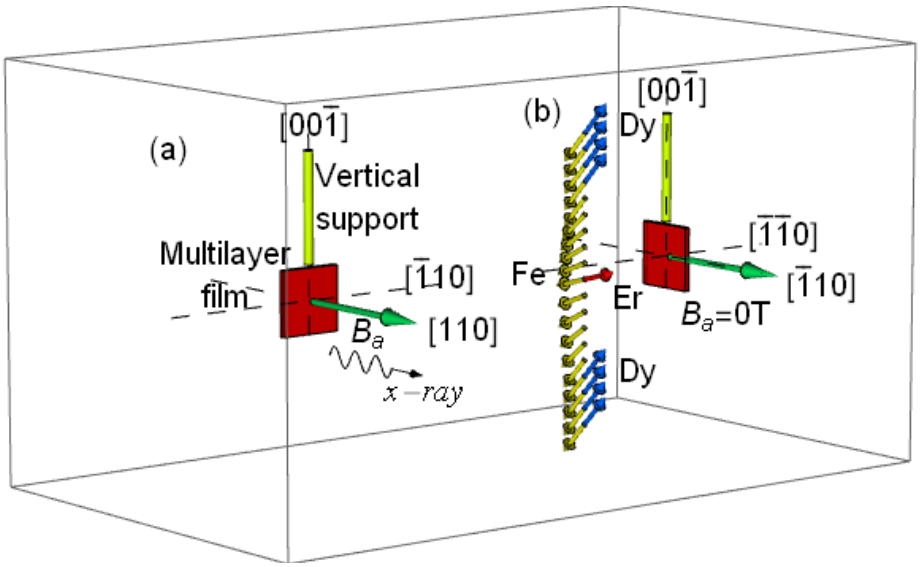

FIG. 2 Schematic diagrams illustrating the two orientations used in the XMCD experiment, with the x-ray beam and field B_a applied along **(a)** the out-of-plane ([110], and **(b)** the in-plane ([$\bar{1}$10])-axis, respectively. Also shown in (b) is a schematic diagram illustrating the AF coupling between the Dy (blue) and Er (red) moments with those of the Fe (yellow). Note that even in zero field, there is an exchange spring present in the Fe sublattice. For the experiments depicted in (b) the film was orientated at a small glancing angle of 7^o, with respect to the x-ray beam.

The resulting Er and Dy loops, for fields applied along the [110] growth-axis, can be seen in Fig. 3(a,b).

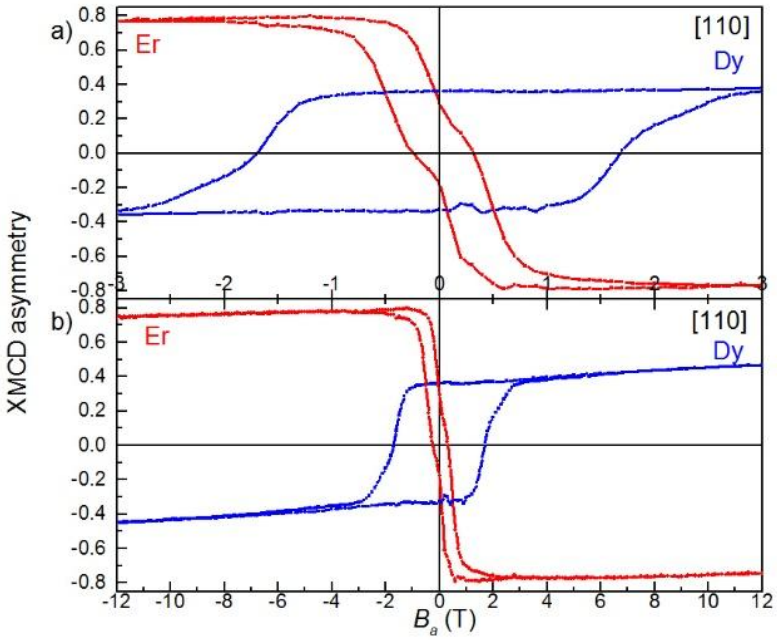

FIG. 3(a,b) Out-of-plane [110]-magnetic loops for the Dy and Er in an Er-doped $DyFe_2/YFe_2$ multilayer at 100 K, measured by XMCD over a field range of ±3 T and ±12 T, respectively.

An examination of these magnetization curves reveals several features. In particular, the Er loop is inverted with respect to that of the Dy. Here the Dy loop follows the *norm* in that the Dy moment is positive in a positive magnetic field. By contrast, the Er moment is negative. Here the sign of the Er moment is dictated by the behaviour of the exchange spring. In a large magnetic field the Fe spins in the center of the YFe_2 springs are roughly parallel to those of the Dy moments. However the Er is AF-coupled to its Fe counterparts. Thus the Er-loop is inverted with respect to that of the Dy. Note also that the coercive field of the Er is much less than that of the Dy. The coercivity of the Er loop is determined primarily by the bending field of the exchange spring, typically ~0.5 T in $DyFe_2(60\text{Å})/YFe_2(240\text{Å})_{15}$ multilayer systems [4,5,6].

For comparative purposes, similar loops for fields applied long the in-plane $[\bar{1}10]$-axis can be seen in Fig. 4(a,b).

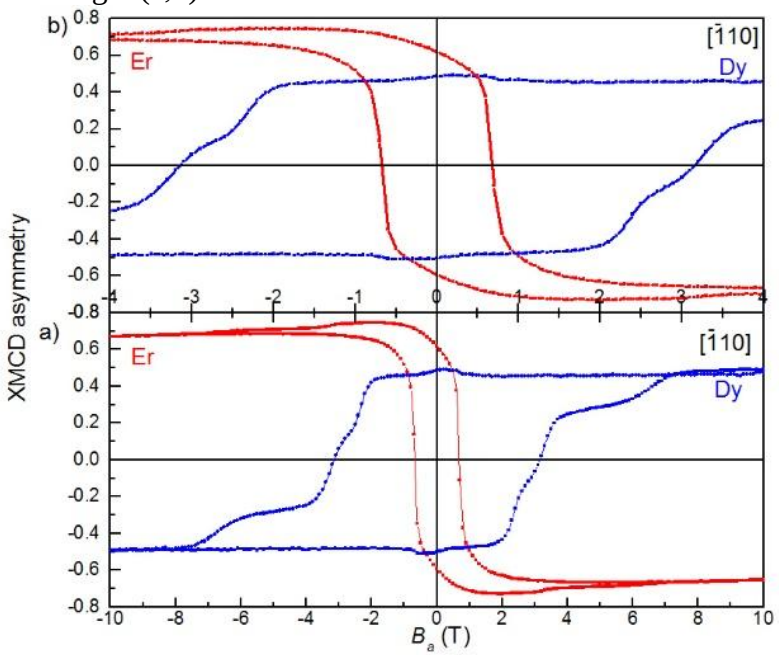

FIG. 4(a,b). In-plane $[\bar{1}10]$-magnetic loops for the Dy and Er in an Er-doped $DyFe_2/YFe_2$ multilayer at 100 K, measured by XMCD over a field range of ±4 T and ±10 T (After Ref. [6]).

On comparing the two magnetization curves for these two seemingly equivalent hard-axes it is apparent that the out-of-plane Er loop of Fig. 3(a) shows a definite inflection at around ±0.5 T, which is not apparent in the in-plane loop of Fig. 4(a). In fact, the latter is an excellent example of 'exchange-spring collapse', as described in Ref. [6].

In this paper we provide an explanation for the differences in Er-switching behavior, for the two seemingly equivalent directions of magnetization. In particular, it will be argued that the inflection point in Fig. 3(a) reveals the existence of a stable exchange state $Dy_B[010]/Er_S[\bar{1}1\bar{1}]$, which we shall refer to as a *stepping stone state* (C2), roughly half way between the maximum and minimum Er Signals. However, its' in-plane counterpart $Dy_B[010]/Er_S[11\bar{1}]$ (B2) is unstable and is bypassed by exchange spring collapse. Schematic diagrams of the two switching mechanisms in question can be seen in Figs. 5 (a,b) for fields applied along the [110] and $[\bar{1}10]$-axes, respectively.

Note that in both cases the Dy moments remain fixed along the [010]-axis, while the Er moments are reversed.

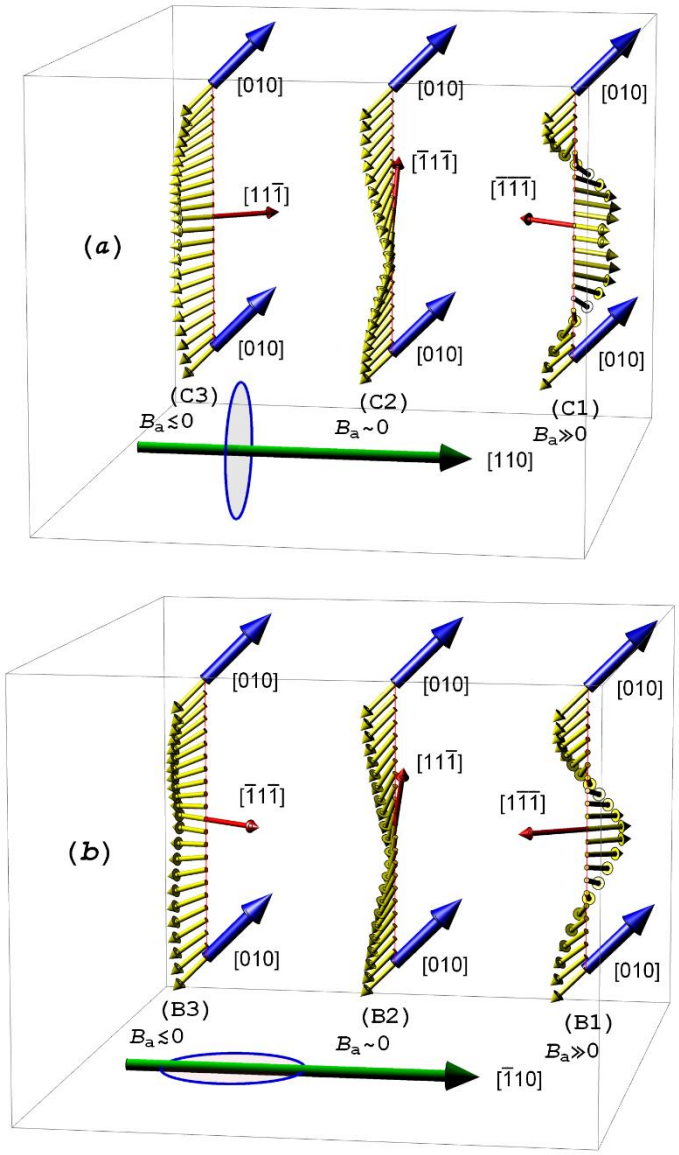

FIG. 5 (a,b). Possible Er switching scenario for fields applied along an out-of-plane [110]-axis (a), and in-plane [$\bar{1}$10]-axis (b), respectively. The nomenclature follows that of Ref. [6]. The subscript B (S) refers to Dy in the *bulk* $DyFe_2$ layer, Er in the *spring*, respectively.

However, before providing an explanation of the switching scenarios sketched out in Figs. 5 (a,b) it is advantageous to examine all possible sources of anisotropy and asymmetry.

3. Cubic crystal-field anisotropy terms

In free standing RFe_2 Laves phase compounds, the principle source of anisotropy arises from the interaction of the 4th and 6th order multipolar charge distributions of the R^{3+} $4f^n$ electrons with high-order electric field gradients. This electrostatic interaction, known as the crystal-field interaction, has been the subject of intense study by

Atzmony *et al.*, [10] and Atzmony and Dariel [11]. The latter used the ^{57}Fe Mossbauer effect to determine the direction of magnetization in a myriad of mixed $R1_xR2_{1-x}Fe_2$ compounds. Subsequently, they interpreted their findings in terms of (*i*) isotropic Fe-Fe and RE-Fe exchange interactions, and (*ii*) a crystal field interaction at the RE site. Indeed, it is the latter which determines the easy axes of magnetization. Specifically, the RE Hamiltonian takes the form:

$$\boldsymbol{\mathcal{H}} = \boldsymbol{\mathcal{H}}_{\mathrm{Ex}} + \boldsymbol{\mathcal{H}}_{\mathrm{CF}} \tag{1}$$

where:

$$\boldsymbol{\mathcal{H}}_{\mathrm{Ex}} = 2(g_J - 1)\mu_{\mathrm{B}} H_{\mathrm{Ex}}^{\mathrm{Fe}} J_{\mathrm{z}} \tag{2}$$

and

$$\boldsymbol{\mathcal{H}}_{\mathrm{CF}} = B_4[\boldsymbol{O}_{40} + 5\boldsymbol{O}_{44}^{C}] + B_6[\boldsymbol{O}_{60} - 21\boldsymbol{O}_{64}^{C}] \tag{3}$$

Here the exchange field $H_{\mathrm{Ex}}^{\mathrm{Fe}}$ is assumed to follow the temperature dependence of the Fe sublattice, as determined by the ^{57}Fe Mössbauer effect, $\boldsymbol{\mathcal{H}}_{\mathrm{CF}}$ is the crystal field interaction, B_4 and B_6 are the temperature dependent crystal-field parameters, $\boldsymbol{O}_{40}$, $\boldsymbol{O}_{44}^{C}$, etc., are the crystal-field operators, defined e.g. by Abragam and Bleaney [12], and all the remaining symbols possess their normal meanings. Following [11], we set $\mu_B H_{Ex}^{Fe}(T = 0\ \mathrm{K}) = 150\ \mathrm{K}$ for all rare earths.

Exactly this approach has been followed by Martin *et al.*, [13] who showed that starting from the Hamiltonian of Eq. (1) the magnetic anisotropy can be expressed in the form:

$$E_A^C = \hat{K}_4(T)\boldsymbol{Y}_4^C + \hat{K}_6(T)\boldsymbol{Y}_6^C + \hat{K}_8(T)\boldsymbol{Y}_8^C + \hat{K}_{10}(T)\boldsymbol{Y}_{10}^C + \hat{K}_{12}(T)\boldsymbol{Y}_{12}^C \tag{4}$$

Here the $\hat{K}_n(T)$ are temperature dependent anisotropy parameters and the $\boldsymbol{Y}_n^C$ are combinations of spherical harmonics which possess cubic symmetry, e.g.:

$$\boldsymbol{Y}_4^C = Y_4^0(\theta,\phi) + \sqrt{\frac{5}{14}}\left(Y_4^4(\theta,\phi) + Y_4^{-4}(\theta,\phi)\right) \tag{5}$$

where (θ,ϕ) are the usual polar angles with the z (x) -axes aligned along the [110] ($[00\bar{1}]$) -axes, respectively. The existence of the higher order terms $\hat{K}_8(T)$ etc. arise from cross terms of the form B_4^2, B_4B_6, and B_6^2. More details can be found in Atzmony and Dariel [11] and Martin *et al.*, [13].

In general, the crystal-field anisotropy of Eq. (4) is the dominant term in the anisotropy. Graphical illustrations of the Dy and Er anisotropy surfaces can be seen in Fig. 1 of Ref. [6]. In particular, the anisotropy of the Dy ions (≈25 K) is about 5 times that of the Er ions at 100 K.

Finally, we note that the anisotropy energy E_A of Eq. (4), which has cubic symmetry, cannot differentiate between in-plane $[\bar{1}10]$ and out-of-plane [110] measurements. To distinguish between both directions we must look to the strain and dipolar terms, discussed in the next sections.

4. Strain terms

In practice, thin films of the RFe$_2$ intermetallic compounds are grown epitaxially on a $(11\bar{2}0)$ sapphire wafer at a temperature of 600°C ,Wang *et al.*, [8]. At this temperature the epitaxial relationship between the sapphire substrate and that of the RFe$_2$ films is fully relaxed [14]. However when the film is cooled down to 300 K, the metallic film

contracts rather more than the sapphire wafer. Thus the MBE-grown films exhibit strain, frozen in during crystal growth. From x-ray studies Mougin *et al*., [14] found that the principal strain is the so-called shear strain characterized by ϵ_{xy}. This term, which has the same form as the magneto-elastic Hamiltonian, is usually written:

$$\boldsymbol{\mathcal{H}}_{\mathrm{ME}} = b_2 \epsilon_{xy} \alpha_x \alpha_y \tag{6}$$

Here b_2 is the temperature dependent magneto-elastic constant, ϵ_{xy} is the shear strain (~–0.55%), and α_x and α_y are the direction cosines with respect to the [100] and [010] cubic axes, respectively. This term can differentiate between in-plane and out-of-plane measurements, given that the [001]-axis is in-plane while the [010]-axis is 45^{o} out of plane (see Fig. 1). More details of the connection between the magneto-elastic Hamiltonian (and additional cross-terms) can be found in Bowden *et al*., [15]. However in passing we note that Zimmermann *et al*., [16] have argued on the basis of fitting their computer simulations with experiment that a better fit is obtained if the $b_2\epsilon_{xy}$ term is increased by a factor of 2.5.

Finally, Bowden *et al*., [15] have shown that this term can be re-expressed in terms of the usual angular momentum operators:

$$\boldsymbol{\mathcal{H}}_{\mathrm{ME}} = \frac{b_2 \epsilon_{xy}}{J(J+1)} \frac{1}{2} \left(J_x J_y + J_y J_x \right) \tag{7}$$

Once again, this extra term in the Hamiltonian gives rise to an additional term in the magnetic anisotropy which takes the form:

$$E_A^{\mathrm{ME}} = \widehat{K}_2(T) \frac{1}{2} \sqrt{\frac{15}{2\pi}} \sin^2\theta \sin 2\phi \tag{8}$$

More details together with temperature dependent values of the anisotropy parameter $\widehat{K}_2(T)$ can be found in Ref. [15].

To probe this source of anisotropy, micromagnetic simulations were carried out using the model described in Ref. [6]. However for the two exchange-spring states in question we find the following stability ranges:

$$\mathrm{Dy_B}[010]/\mathrm{Er_S}[\bar{1}1\bar{1}] : -0.3584 \leq B_z \leq +0.9843 \text{ T} \tag{9}$$

$$\mathrm{Dy_B}[010]/\mathrm{Er_S}[11\bar{1}] : -0.4343 \leq B_y \leq +1.214 \text{ T} \tag{10}$$

Here B_z (B_y) is shorthand for fields applied along the [110] ($[\bar{1}10]$) axes, respectively. From these calculations, performed in the absence of dipolar interactions, it is evident that while there is a small asymmetry in the stability range of these two exchange spring states, the difference is too small to provide an explanation for the apparent absence of the $\mathrm{Dy_B}[010]/\mathrm{Er_S}[11\bar{1}]$ spring state (B2) in Fig. 4(b). We are obliged therefore to look for another anisotropic term in the energy of the magnetic exchange spring system. As seen in the next section, long-range dipolar fields can distinguish between the two exchange spring states in question.

5. The long-range dipole-dipole interaction

It has long been known that long-range dipolar fields in thin magnetic films can shift the ferromagnetic resonance (FMR) significantly away from the simple Zeeman relationship: $\omega = \gamma B_a$. For fields applied in-plane, the resonance is shifted to $\omega = \gamma\sqrt{B_a(B_a + \mu_0 M)}$, where B_a and M are the applied field and magnetization of the film, respectively, Kittel [18,19]. In elemental Fe $\mu_0 M \approx 2.2\,T$, so that the shift is appreciable. In general, this problem is usually discussed in terms of the

demagnetizing fields for a thin film. Here the internal field seen by the individual moments is given by: $B = B_a - DM$, where $D = -1\,(0)$ for fields applied perpendicular (parallel) to the plane of the film, respectively. This information alone is enough to generate the Kittel formula given above.

Next we observe that the $DyFe_2(60\,\text{Å})/YFe_2(240\,\text{Å})_{15}$ film in question has been specifically engineered to give a net magnetic moment $M \approx 0$, in zero field. The net magnetic moment of a given YFe_2 layer almost cancels out that of its' neighboring $DyFe_2$ layer, leading to a layered net antiferromagnet with an estimated $\mu_0 M \approx 0.2\,T$. At first sight therefore, demagnetizing fields should only play a small role in determining the dynamics/statics of the 4000 Å thick film. However as we shall demonstrate below, despite the low net magnetic moment of the film, dipolar fields in man-made layered multilayers are far from negligible and reflect the symmetry of the multilayer. Some idea of the importance of these fields can be gained by examining the magnetization of the individual layers. We find $\mu_0 M(DyFe_2) \approx 1.5\,T$ and $\mu_0 M(YFe_2) \approx 0.7\,T$, at $T \approx 100$ K. These values are appreciable, so the potential for a periodic variation in dipolar field strength is high.

To put these arguments on a quantitative footing, we use an alternative approach to calculate dipolar-field shifts. Specifically, the field at a given site is augmented by dipolar fields generated by all the dipoles in the film. This approach, which has a distinguished history in the field of magnetism, has recently been revisited by Ref. [20]. Here the dipolar fields at a given site are calculated layer-by-layer, with the sole proviso that all the spins within a given monolayer in the film are parallel. With this assumption, the local dipolar field $\boldsymbol{B}_{\rm DS}(k)$ at a given site in the $k^{\rm th}$ plane arising from all the spins in the k' plane can be expressed in the form:

$$\boldsymbol{B}_{\rm DS}(k) = \frac{\mu_0}{4\pi a^3}\begin{pmatrix} D_{xx}^{\Delta k} & 0 & 0 \\ 0 & D_{xx}^{\Delta k} & 0 \\ 0 & 0 & -2D_{xx}^{\Delta k} \end{pmatrix}\begin{pmatrix} \mu_x^{k'} \\ \mu_y^{k'} \\ \mu_z^{k'} \end{pmatrix} \tag{11}$$

where $\Delta k = k - k'$. In thin films with a large aspect ratio and a simple cubic lattice we find the dimensionless numbers:

$$\begin{aligned} D_{xx}^{0} &= 4.516811 \\ D_{xx}^{\pm 1} &= -0.1637329 \\ D_{xx}^{\pm 2} &= -0.000278402 \end{aligned} \tag{12}$$

the rest being negligible. In what follows, we drop the $D_{xx}^{\pm 2}$ term since only the in plane and next nearest plane dipolar contributions are important. For the $k^{\rm th}$ plane therefore we write:

$$\epsilon_{\rm dip}^{k} = -\boldsymbol{\mu}_k.\left(\boldsymbol{B}_{\rm DS}(k) + \boldsymbol{B}_{\rm DS}(k+1) + \boldsymbol{B}_{\rm DS}(k-1)\right)$$

$$= -\frac{\mu_0 \mu_B^2}{4\pi a^3}\begin{pmatrix} (\mu^k)^2 D_{xx}^0(1 - 3\cos^2\theta_k) \\ +\mu^k \mu^{k+1} D_{xx}^1\left(\sin\theta_k \sin\theta_{k+1}\cos\left(\phi_{k+1} - \phi_k\right) - \cos\theta_k\cos\theta_{k+1}\right) \\ +\mu^k \mu^{k-1} D_{xx}^1\left(\sin\theta_k \sin\theta_{k-1}\cos\left(\phi_{k-1} - \phi_k\right) - \cos\theta_k\cos\theta_{k-1}\right) \end{pmatrix} \tag{13}$$

where the magnetic moments μ^k are given in Bohr magnetons. Finally, note that because $D_{xx}^0 \gg D_{xx}^1$ the dominant term is simply:

$$\epsilon_{\rm dip}^{k}\left(\theta_k, \phi_k\right) \approx -\frac{\mu_0 \mu_B^2}{4\pi a^3}\left((\mu^k)^2 D_{xx}^0(1 - 3\cos^2\theta_k)\right) \tag{14}$$

Thus the effect of the long-range dipolar fields is very much like that of a single-ion anisotropy tending to align the spins in-plane. Note that this term is driven by the dipoles in the *same* plane and scales with $(\mu^k)^2$. In practice therefore, this dipolar source of anisotropy will be in competition with the crystal-field interaction at the rare-earth sites. However, in those situations where the Dy moments lie along an in-plane [001] easy-axis of magnetization, the dipolar field anisotropy and the Dy crystal-field interaction will act in unison. However, in the case of the Er moments, where the crystal-field interaction prefers out-of-plane <111> type easy-axes (see Fig. 1), competition between the crystal-field interaction and dipolar fields can occur.

We are now in a position to distinguish qualitatively between the two states in question. First, consider the stepping stone state $Dy_B[010]/Er_S[\bar{1}1\bar{1}]$ (see Fig. 4) which occurs in the out-of-plane [110]-data of Fig. 2(a). Here, we observe that the $[\bar{1}1\bar{1}]$ axis is an easy in-plane axis for the crystal-field interaction at the Er site (see Fig. 1). So both the long-range dipolar anisotropy arising from the $ErFe_2$ layers themselves and the Er crystal field interaction act in unison. However this is not the case for the $Dy_B[010]/Er_S[11\bar{1}]$ state with the field applied in-plane (see Fig. 5). Here the crystal-field interaction demands that the Er ions point out-of-plane, while the dipolar forces require in-plane. For this state, therefore, competition will occur leading to a decrease in the depth of the potential well available to the Er ion. Thus in practice, it should not come as a surprise that this state is either unstable or is characterized by a small stability range. In the next section, estimates are given for the strength of the dipolar interaction in RFe$_2$ intermetallic compounds.

6. Dipolar field estimates

The micromagnetic model used here and in earlier work has already been described in Refs. [6,21]. However, despite its successes, this model is a great simplification of the actual situation. For example, the unit cell used in the micromagnetic model can be seen in Fig. 6(a). Here the R moments (say 10 μ_B) and the two Fe moments (say 2□1.5 μ_B) are shown at single sites, in a cubic cell of $(a/2)^3$, where a is the size of the unit cell (a = 7.321 Å for $DyFe_2$). In reality, there are 8 R ions and 16 Fe ions per unit cell a^3 of the cubic Laves phase, as shown in Fig. 6(b). The reason for choosing the unit cell of Fig. 5(a) is (*i*) to simplify the micromagnetic model [4-6, 20] and importantly (*ii*) to conserve the magnetization M of the RFe$_2$ compounds.

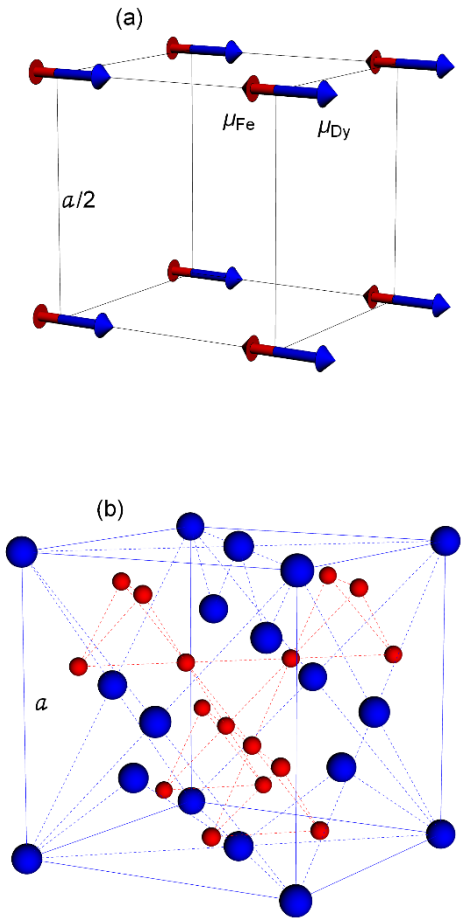

FIG.6 (a). Simple cubic model for the *R*Fe$_2$ compounds (after Ref. [21]). The spacing is $a/2$, where a denotes the size of the real unit cell. **(b)** Actual unit cell. Here the blue (red) spheres represent R (Fe)-ions, respectively, and a = 7.321 Å for DyFe$_2$.

From a comparison of Figs. 6(a,b) it is clear that one should be concerned when using the simple cubic (SC) model of Fig. 6(a) to replicate the actual dipolar fields in the *R*Fe$_2$ compounds. At best, estimates obtained with the SC model should be treated as a guide. Nonetheless, most would agree that in thin films, demagnetizing fields generated by free poles on the top and bottom of the film tend to align the moments in-plane. However, it is stronger than that. In Ref. [20], it is shown that dipolar fields generated within each individual plane tend to align moments in-plane. So with the above provisos, we set:

$$\epsilon_{\rm dip}^{k}(\theta_k,\phi_k) = -D\begin{bmatrix} (\mu^k)^2(1-3\cos^2\theta_k) \\ +\eta\mu^k\mu^{k+1}\left(\sin\theta_k\sin\theta_{k+1}\cos\left(\phi_{k+1}-\phi_k\right)-\cos\theta_k\cos\theta_{k+1}\right) \\ +\eta\mu^k\mu^{k-1}\left(\sin\theta_k\sin\theta_{k-1}\cos\left(\phi_{k-1}-\phi_k\right)-\cos\theta_k\cos\theta_{k-1}\right)\end{bmatrix} \quad (14)$$

where

$$D = -\frac{\mu_0\mu_B^2}{4\pi(a/2)^3k}D_{xx}^0 = 0.01260\ (\mathrm{K})$$
$$\eta = \frac{D_{xx}^1}{D_{xx}^0} = -0.03625 \quad (15)$$

with D given in Kelvin. We remind that the principle contribution to the dipolar field arises from *in-plane* moments ($k^{\rm th}$ plane), with more modest contributions from the next nearest $k\pm1$ planes.

Turning now to the stepping stone state $\mathrm{Dy_B}[010]/\mathrm{Er_S}[\bar{1}1\bar{1}]$ we find that the range of stability is extended by the inclusion of the dipolar anisotropy:

$$\mathrm{Dy_B}[010]/\mathrm{Er_S}[\bar{1}1\bar{1}]: \; -1.4995 \leq B_z \leq +1.9574 \text{ T} \qquad (16)$$

This represents an increase in field range of 1.34 to 3.47 T [c.f. Eqs. (9) and (16)]. As expected therefore inclusion of the dipole-dipole interaction strengthens the stepping stone state. By contrast, the range of stability for the counterpart $\mathrm{Dy_B}[010]/\mathrm{Er_S}[11\bar{1}]$ state (B2) is much reduced by the inclusion of the dipole term. For example, on halving the strength of the dipolar terms we find:

$$\mathrm{Dy_B}[010]/\mathrm{Er_S}[11\bar{1}]: \; 0.1336 \leq B_y \leq +0.8015 \text{ T} \qquad (17)$$

This represents a reduction in field range from 1.65 to 0.67 T (c.f. Eqs. (10) and (17)). Moreover, the range is reduced to zero, by increasing the strength of the dipolar term towards its full (estimated) value.

In summary therefore, the existence of the stepping-stone-state C2 in Fig. 5(a), coupled with the absence of the stepping-stone-state B2 in Fig. 5(b), constitute strong evidence for the existence of an appreciable dipolar contribution to the anisotropy of the Er sites in the $ErFe_2$ planes. In the following section, it is also argued that this is also true for the Dy moments in the $DyFe_2$ bulk layers.

7. The coercivity of the hard Dy layer

In general, the inclusion of the dipolar terms will have a minor effect on the Fe moments in the YFe_2 layers. Here the dipolar energy scales as: $\mu_{\mathrm{Fe}}^2 = 9\,\mu_{\mathrm{B}}^2$ at $T = 0$ K, giving rise to a dipolar splitting ~0.1 K. However in the RFe_2 layers dipolar splitting is much larger. In the $DyFe_2$ layers we have $\left(\mu_{\mathrm{Dy}} - \mu_{\mathrm{Fe}}\right)^2 = 49\,\mu_{\mathrm{B}}^2$ at $T = 0$ K, giving rise to a dipolar field splitting ~0. 5 K (alternatively, in units of a magnetic field: ~0.74 T). Thus the essentially planar dipolar anisotropy should play a role in determining the coercive field of the Dy layers. This does appear to be the case. If we define the coercive field as that field at which the Dy XMCD signal goes to zero, we find $B_C = 1.8$ T for the out-of-plane measurements [see Fig. 2(a)], and $B_C = 3.5$ T for the in-plane measurements [see Fig. 4(a)]. Thus the coercivity of the Dy loop, taken along seemingly equivalent $[\bar{1}10]$ and [110]-directions, points, once again, to the importance of including dipole-dipole terms into the micromagnetic model.

8. Discussion and Conclusions

In this paper, results have been presented and discussed for Er-doped (110)-oriented $\mathrm{DyFe_2(60\,\text{Å})/YFe_2(240\,\text{Å})_{15}}$ multilayer films, at 100 K in fields of up to ±12 T. In general, the films are characterized by low (high) coercivity Er (Dy) loops. In particular, switching mechanisms have been proposed for the low coercivity Er loop, in fields applied along seemingly equivalent hard-magnetic [110]-type axes. Differences between in-plane $[\bar{1}10]$ and out-of-plane [110] results have been identified. In particular, the out-of-plane Er results reveal the existence of a stepping stone exchange-spring state $\mathrm{Dy_B}[010]/\mathrm{Er_S}[\bar{1}1\bar{1}]$ (C2), while its in-plane counterpart $\mathrm{Dy_B}[010]/\mathrm{Er_S}[11\bar{1}]$ (B2) appears to be either weakly stable or unstable. This difference has been attributed to competition between the crystal field and long range, essentially planar, dipole-dipole interactions at the Er site. For the $\mathrm{Dy_B}[010]/$

$Er_S[\bar{1}1\bar{1}]$ stepping-stone-state, both the crystal-field and dipolar interactions re-enforce each other, however, for the $Dy_B[010]/Er_S[11\bar{1}]$ state the situation is otherwise. In addition, the coercive field of the Dy-loop, for both out-of-plane and in-plane, again points to the importance of including the essentially planar anisotropy arising from dipole-dipole interactions, even in films where the net magnetization is zero. Finally, we stress that the existence of the new magnetic exchange spring state $Dy_B[010]/Er_S[\bar{1}1\bar{1}]$ would be impossible to identify without the use of element-selective x-ray magnetic circular dichroism (XMCD) experiments, especially given that the $ErFe_2$ layers account for just ~1% of the sample.

Acknowledgements

We acknowledge Diamond Light Source for time on beamline I10 under proposals SI-8213 and SI-13758.

References

1. D. Weller and A. Moser, IEEE Trans. Magn. **35**, 4423 (1999). *Thermal effect limits in ultrahigh-density magnetic recording.*

2. D. Suess, T. Schrefl, R. Dittrich, M. Kirschner, F. Dorfbauer, G. Hrkac, and J. Fidler, J. Magn. Magn. Mater. **290-291**, 551 (2005). *Exchange spring recording media for areal densities up to 10Tbit/in^2*.

3. P. Krone, D. Makarov, T. Screfl, and M. Albrecht, Appl. Phys. Lett. **97,** 082501 (2010). *Exchange coupled composite bit patterned media.*

4. G. B. G. Stenning, G. J. Bowden, S. A. Gregory, J.-M. Beaujour, P. A. J. de Groot, G. van der Laan, L. R. Shelford, P. Bencok, P. Steadman, A. N. Dobrynin, and T. Hesjedal, Appl. Phys. Lett., **101**, 072412 (2012). *Magnetic reversal in a YFe_2 dominated $DyFe_2/YFe_2$ multilayer film.*

5. G. B. G. Stenning, G. J. Bowden, P. A. J. de Groot, G. van der Laan, A. I. Figueroa, P. Bencok, P. Steadman, and T. Hesjedal, Phys. Rev. B **91**, 104404 (2015). *Magnetic reversal in Dy-doped in $DyFe_2/YFe_2$ superlattice films*.

6. G. B. G. Stenning, G. J. Bowden, P. A. J. de Groot, G. van der Laan, A. I. Figueroa, P. Bencok, P. Steadman, and T. Hesjedal, Phys. Rev. B **92,** 104404 (2015). *Exchange spring switching in Er-doped $DyFe_2/YFe_2$ magnetic thin films*.

7. L. R. Shelford, Y. Liu, U. Al-Jarah, P. A. J. de Groot, G. J. Bowden, R. C. C. Ward, and R. J. Hicken, Phys. Rev. Lett. **113,** 067601 (2014). *Ultrafast Optical Parametric Pumping of Magnetization Reorientation and Precessional Dynamics in $DyFe_2/YFe_2$ Exchange Springs.*

8. C. Wang, A. Kohn, S. G. Wang, and R. C. C. Ward, J. Phys.: Condens. Matter **23,** 116001 (2011). *Interlayer diffusion studies of a Laves phase exchange spring superlattice.*

9. G. van der Laan and A. I. Figueroa, Coord. Chem. Rev. **277-278**, 95 (2014). *X-ray magnetic circular dichroism - a versatile tool to study magnetism.*

10. U. Atzmony, M. P. Dariel, E. R. Bauminger, D. Lebenbaum, I. Nowik, and S. Ofer, Phys. Rev. B **7**, 4220 (1973) *Spin-orientation diagrams and magnetic anisotropy of rare-earth-iron cubic Laves compounds.*

11. U. Atzmony and M. P. Dariel, Phys. Rev. B **13**, 4006 (1976), *Non major cubic symmetry axes of easy magnetization in rare-earth-iron Laves compounds*.

12. A. Abragam and B. Bleaney (1970) *Electron paramagnetic resonance of transition ions*, Oxford University Press.

13. K. N. Martin, P. A. J. de Groot, B. D. Rainford, K. Wang, G. J. Bowden, J. P. Zimmermann, and H. Fangohr, J. Phys.: Condens. Matter **18,** 459 (2006), *Magnetic anisotropy in the cubic Laves $REFe_2$ intermetallic compounds*.

14. A. Mougin, C. Dufour, K. Dumesnil, N. Maloufi, Ph. Mangin, and G. Patrat, Phys. Rev. B **59** 5950 (1999), *Strain in single-crystal $RFe_2(110)$ thin films (R=Y, Sm, Gd, Tb, $Dy_{0.7}Tb_{0.3}$, Dy, Er, Lu).*

15. G. J. Bowden, P. A. J. de Groot, B. D. Rainford, K. Wang, K. N. Martin, J. P. Zimmermann, and H. Fangohr, J. Phys.: Condens. Matter **18,** 5861 (2006), *Magnetic anisotropy terms in [110] MBE-grown $REFe_2$ films involving the strain term ϵ_{xy}*.

16. J. P. Zimmermann, K. Martin, G. Bordignon, M. Franchin, R. C. C. Ward, G. J. Bowden, P. A. J. de Groot, and H. Fangohr, J. Magn. Magn. Mater. **321**, 2499 (2009), *Magnetic switching modes for exchange spring systems $ErFe_2/YFe_2/DyFe_2/YFe_2$ with competing anisotropies*.

17. D. Wang, A. R. Buckingham, G. J. Bowden, R. C. C. Ward and P. A. J. de Groot, Materials Research Express **1**, 036110 (2014), *Engineering irreversibility of exchange springs in antiferromagnetic $DyFe_2/YFe_2$ superlattices*.

18. C. Kittel, Phys. Rev. **73**, 155 (1948), *On the theory of ferromagnetic resonance absorption*.

19. C. Kittel (1971) *Introduction to Solid State Physics*, IVth Edition, John Wiley & Sons.

20. G. J. Bowden, G. B. G. Stenning, and G. van der Laan, J. Magn. Magn. Mater. **416,** 449 (2016), *Asymptotic behavior of local fields in thin films*.

21. G. J. Bowden, K. N. Martin, B. D. Rainford, and P. A. J. de Groot, J. Phys.: Condens. Matter **20**, 015209 (2008), *Modelling magnetic exchange springs in 1D, 2D, and 3D.*